RSC Advances




ROYAL SOCIETY OF CHEMISTRY

www.rsc.org/advances

Journal Name

ARTICLE

# Heterojunction $Cr_2O_3$/CuO:Ni photocathodes for enhanced photoelectrochemical performance

Siti Nur Farhana Mohd Nasir,[a*] Mohd Khairul Najib Yahya,[b] Norfaizzatul Wahidah Mohamad Sapian,[b] Norasikin Ahmad Ludin[a], Mohd Adib Ibrahim[a], Kamaruzzaman Sopian[a] and Mohd Asri Mat Teridi[a*]

Received 00th January 20xx,
Accepted 00th January 20xx

DOI: 10.1039/x0xx00000x

www.rsc.org/

Heterojunction p-type photoelectrode consist of chromium oxide, $Cr_2O_3$ and copper oxide, CuO-doped nickel, Ni were prepared using aerosol-assisted chemical vapour deposition (AACVD) and spin-coating. All samples were photoresponsive and showed photocathodic current in 0.5 M $Na_2SO_4$ under simulated solar illumination. The photocathode with optimal composition of 3 layers of CuO and 0.5 % Ni showed enhanced photoactivity relative to bare $Cr_2O_3$. Based on the optical characterization and the flatband potentials calculation, the fabricated $Cr_2O_3$, $Cr_2O_3$/CuO and $Cr_2O_3$/CuO:Ni can absorb visible light that allow water reduction reaction. Moreover, the electrochemical impedance spectroscopy revealed that the charge transfer resistance of $Cr_2O_3$/CuO:Ni was decreased. Thus, in heterojunction structure, the photogenerated electrons in $Cr_2O_3$ are transferred to CuO:Ni layer which then contribute to high photoactivity. The combined advantages of the two strategies (heterojunction and doping) provide favourable charge transport characteristics of the materials.

## Introduction

Investigation of photoelectrochemical (PEC) water splitting has long been studied for renewable energy sources. Particularly, the study is focussed on semiconductor materials which have great potential to split water molecule into oxygen and hydrogen gas. Metal oxides have been chosen for decades to drive photocatalytic reaction. However, one major problem may arise from using metal oxides. Most of the metal oxides have wide bandgap energy which cannot utilize sufficient solar photons to split water efficiently unless modifications are made to these photoelectrodes.[1] Several attempts include nanostructure morphology control,[2,3] substitutional doping of metal cations [4,5] and formation of heterojunction[6,7] have been made to address this limitation in order to improve the photoelectrochemical performance. In contrast to a single component photocatalyst, heterojunction of two semiconductors has been recognized as an attractive solution to create high efficiency device by extending the light absorption. It can combine merits of each component to show synergistic effects.[8,9] Additional benefit can be expected by creating a junction structure that can enhance electron-hole separation preventing energy loss during electron transfer in the electrolyte.[10] Ever since the pioneering work of n-type $TiO_2$ electrode by Fujima and Honda[11], numerous studies have primarily concentrated on n-type metal oxide semiconductors such as $BiVO_4$,[12-15] $Fe_2O_3$[16-19] and $WO_3$[20-23] in photoelectrolysis. On the other hand, research efforts in the p-type semiconductor photoelectrode materials such as $Co_2O_3$,[24,25] NiO,[26-27] $Cr_2O_3$[7,28] and CuO[29,30] have been seldom reported. Among these materials, $Cr_2O_3$ and CuO are the most promising materials to be applied in photoelectrodes. $Cr_2O_3$ has been studied extensively in the field of photocatalytic,[31] homogeneous catalysis,[32] and hydrogen absorption.[33] Under visible light irradiation, $Cr_2O_3$ exhibited weak photocatalytic activity due to wide bandgap energy (3.45 eV)[31] which allows this material only to be activated by UV light. Therefore, the formation of heterojunction with matching band potentials is expected to improve the photo-conversion efficiency of photogenerated charge carriers. For p-type photoelectrode material, CuO with narrow bandgap energy (1.4-1.8 eV) was found to be much more active under visible light and has suitable band position for water reduction reaction ($H^+$ to $H_2$).[4,34-37] Aside from that, CuO has long been a candidate as a photocathode because of several reasons including low production cost, natural abundance, non-toxic material, good electrical properties and more importantly it can produce faster electron transfer compared to other photocatalysts.[38]

In the past years, some metal oxide semiconductors have been modified by forming junction structure to promote efficient electron-hole separation. For example, the ZnO/CuO heterojunction branched nanowires photoelectrodes was found to exhibit higher photocurrent due to broadband photoresponse from UV to near IR region.[39] Recently, it was shown that higher photocatalytic activity could be obtained from CuO/$TiO_2$ heterojunction. The performance enhancement are attributed to the photoelectron transfer from the more negative conduction band of $TiO_2$ to CuO.[40] On top of that, due to the relatively high resistance of CuO, the movement of

[a] Solar Energy Research Institute (SERI), Universiti Kebangsaan Malaysia, 43600 Bangi, Selangor, Malaysia.
[b] School of Applied Physics, Universiti Kebangsaan Malaysia, 43600 Bangi, Selangor, Malaysia.
Corresponding Author E-mail: farhanaana98@gmail.com and asri@ukm.edu.my.
Fax: +603 8911 8574; Tel: +603 8911 8580
Electronic Supplementary Information (ESI) available: See DOI: 10.1039/x0xx00000x

photon-excited electrons to the electrode and electrolyte interface may be limited.[41] Hence, to reduce the resistance of CuO, and to improve the photo-responsiveness of CuO is by doping with metal ions.[41] Doping the impurity metal ions with semiconductor is a useful technique to change the electrical, magnetic and optical properties of the material.[42] Recently, Ni has received increased interest as a dopant in the studies of thin films.[43,44,45] In previous work, the electronic properties of CuO was altered when doping with Ni. The increase in photocurrent density and conductivity by 0.76 % and 1.5 % respectively was realized after 2 % of Ni concentration was added as a dopant into CuO.[5] Therefore, we can say that incorporation of Ni ion into CuO nanostructure can affect the conductivity of the host material depending on the amount of dopant inserted. Herein, we applied both concepts of heterojunction and doping as useful approach to enhance the photoelectrochemical properties. First, we fabricated the heterojunction $Cr_2O_3$/CuO thin film photocathodes through AACVD and spin-coating. In a separate experiment, Ni dopant was added into CuO sol-gel which later coated on $Cr_2O_3$ through spin-coating. These two strategies were combined together in order to have better utilization of solar irradiation to improve the photocatalytic activity. Structural characterizations and photoelectrochemical behavior of the fabricated samples are also examined.

## Experimental

### Deposition of $Cr_2O_3$ thin films by AACVD

Conducting glass of fluorine-doped tin oxide (FTO, TEC 8, ~8Ω/sq Pilkington) was cleaned with acetone, iso-propanol and deionized water for 15 minutes respectively in the ultrasonic bath and dried in air. To prepare $Cr_2O_3$ by AACVD, modification of previously published method was employed.[12] An ultrasonic dehumidifier was used to generate the aerosol from a mixture of 50 mM chromium (III) acetylacetonate, $Cr(C_5H_7O_2)_3$ in 100 ml toluene which was then transported by a carrier gas to the heated substrate (~ 460 °C). The deposition time was optimized from 15, 30, 45 and 60 minutes. The as-deposited $Cr_2O_3$ thin films are greenish, uniform and adhere strongly onto the FTO substrate as tested by "scotch tape test".

### Synthesis of sol-gel Ni-doped CuO solution

All the CuO layers were prepared based on a previously published method with some modifications.[30] To prepare 0.3 M CuO sol, copper (II) acetate monohydrate, $Cu(CO_2CH_3)_2.H_2O$ was added in ethanol under vigorous stirring for 20 minutes. At this time, diethanolamine was dripped slowly until the solution was completely dissolved. Subsequently, minimum amount of propylene glycol was added into the solution and then stirred for 60 minutes. The solution was allowed to age for 2 days at room temperature. 10 mM nickel (II) nitrate hexahydrate, $Ni(NO_3)_2.6H_2O$ in minimum amount of ethanol was prepared as dopant. Then, 0.25 %, 0.5 % and 1 % of Ni solution was dripped into CuO sol and stirred in ultrasonic bath before use.

### CuO: Ni layer deposition

The as-prepared CuO and CuO:Ni sol were spin coated (1500 rpm, 25 seconds) onto $Cr_2O_3$ films and then dried in air at 100 °C for 15 minutes for each coating to remove the organic solvent. This process was repeated three times before the substrates were subjected to a final thermal annealing at 450 °C for 1 hour.

### Materials Characterization

### Structural and optical characterizations

X-ray diffraction (XRD) spectra were obtained using (model Bruker D8 Advance) in the range from 20 to 60°. The average grain size of the samples was calculated based on the following Scherer's equation:

$$Grain\ size = \frac{k\lambda}{\beta cos\theta}$$

where, λ is the X-ray wavelength of 0.15406 nm, β is the full width at half-maximum (FWHM) at (110) for $Cr_2O_3$ and (111) for $Cr_2O_3$/CuO and $Cr_2O_3$/CuO:Ni respectively, θ is the Bragg angle, and k is a constant. The surface roughness and topographic images of thin films were identified using NanosurfeasyScan 2 Atomic Force Microscopy (AFM). For ultraviolet-visible spectroscopy (UV-Vis) absorbance studies, samples were measured using PerkinElmer UV/VIS/NIR spectrophotometer Lambda 950. The thin films morphology was characterized using a field-emission scanning electron microscope (FESEM) and energy dispersive X-ray spectroscopy (EDX) on (FE-SEM SUPRA VP55).

### Photoelectrochemical (PEC) measurements

The steady state photocurrent density, electrochemical impedance spectroscopy (EIS) as well as Mott-Schottky analysis were performed in a 3-electrodes configuration consisting of SCE (saturated KCl) as reference electrode, a Pt plate as the counter electrode, and the $Cr_2O_3$, $Cr_2O_3$/CuO, $Cr_2O_3$/CuO:Ni thin films as working electrodes. The samples were measured in 0.5 M $Na_2SO_4$ aqueous electrolyte solution with 1 $cm^2$ of active area. A Metrohm potentiostat / galvanostat Autolab PGSTAT 204 was used to supply the desired potential and frequency to the electrodes. The measurements were conducted under dark, chopped and light conditions with a xenon lamp (light intensity of 100 $mWcm^{-2}$). The EIS and Mott-Schottky characterizations were performed using the same experimental setup as above. The applied frequency for EIS was 100 kHz-10 mHz under dark and illumination. The Mott-Schottky plots were performed in the absence of light at -0.5 to 0.4 V *vs*. SCE.

## Results and Discussion

### Structural properties

Structural characteristic of the as-deposited $Cr_2O_3$, $Cr_2O_3$/CuO and $Cr_2O_3$/CuO:Ni films analysed using X-ray diffraction are presented in figure 1. For $Cr_2O_3$ (figure 1a), the peaks at 24.5°, 33.6°, 36.2°, 41.5°, 50.2° and 54.8° correspond to (012), (104), (110), (113), (024) and (116) planes. All the $Cr_2O_3$ peaks on the XRD pattern can be indexed to the rhombohedral structure (JCPDS 70-3765). After CuO was

coated upon the $Cr_2O_3$ layer (figure 1b), new peaks are observed at 32.5°, 35.6°, 38.8° and 48.7°. These peaks are attributed to (110), (-111), (111) and (-202) planes which represent CuO base-centered monoclinic structure (JCPDS 73-6023). The XRD pattern of the $Cr_2O_3$/CuO:Ni (figure 1c) has the same crystal structure to that $Cr_2O_3$/CuO except that the new peaks of Ni appear at planes (111) and (200). The other peaks shown to have no significant changes suggesting that the mass loading of Ni is very small. In addition, the reduction of grain size observed in Table 1 is attributed to the lattice distortion induced by Ni doping.[46] From XRD, the formation of $Cr_2O_3$, CuO and Ni were confirmed and no impurity peaks were detectable.

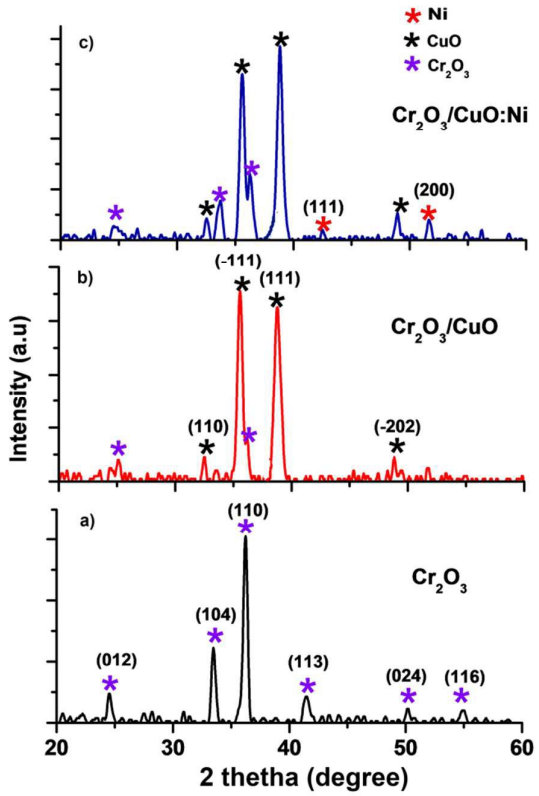


**Figure 1**: XRD patterns of (a) $Cr_2O_3$, (b) $Cr_2O_3$/CuO and (c) $Cr_2O_3$/CuO:Ni thin films.

**Atomic Force Microscopic (AFM)**

Surface roughness and grain size of each sample were compared and presented in table 1. Figure 2 displays the 3D view of the thin films. Although the AFM images show less noticeable changes in thin films topology, $Cr_2O_3$/CuO:Ni recorded the highest surface roughness and smallest grain size compared to $Cr_2O_3$ and $Cr_2O_3$/CuO. Hence, this indicate that the formation of CuO:Ni layer onto $Cr_2O_3$ alter the topology of the films. Generally, high surface roughness and small grain size can significantly affect the PEC performance as more sites are exposed in the photocatalytic reaction. It was found that the grain size of the films decreased in the presence of Ni. The reduction of grain size is attributed to the substitution of $Ni^{2+}$ (0.69 Å) with $Cu^{2+}$ (0.73 Å) onto CuO lattice which further caused the lattice distortion and change in ionic radii.[45]

Table 1: Surface roughness (obtained from AFM), grain size (calculated from XRD) and particle size (taken from FESEM) of $Cr_2O_3$, $Cr_2O_3$/CuO, and $Cr_2O_3$/CuO:Ni thin films.

| Samples | Grain size (Å) | Surface roughness (nm) | Particle size (nm) |
|---|---|---|---|
| $Cr_2O_3$ | 453.10 | 45.64 | 840.00 |
| $Cr_2O_3$/CuO | 283.90 | 49.59 | 94.12 |
| $Cr_2O_3$/CuO:Ni | 209.60 | 54.56 | 58.83 |

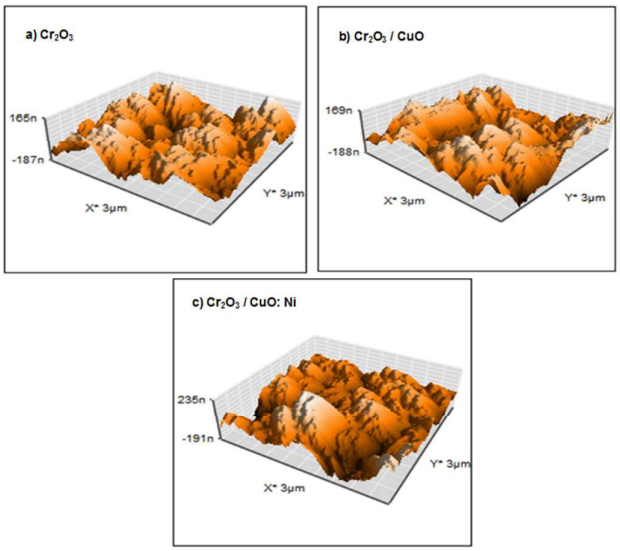


**Figure 2**: AFM images of (a) $Cr_2O_3$, (b) $Cr_2O_3$/CuO and (c) $Cr_2O_3$/CuO:Ni thin films.

**Morphological properties**

Elemental and topographical characteristic of the thin films were carried out through Field Emission Scanning Electron Microscopy and the result are shown in figure 3.

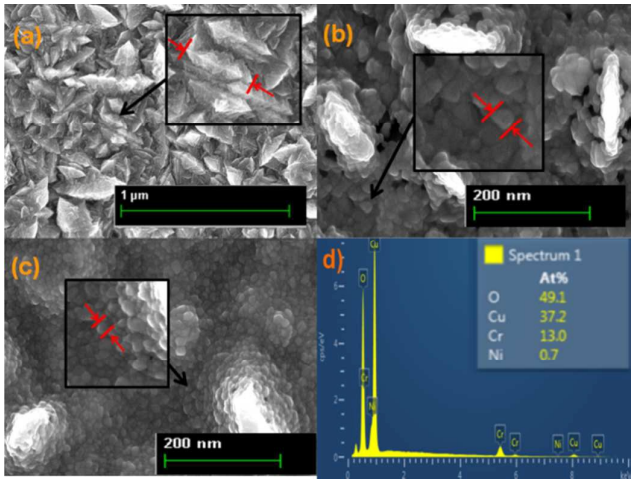

**Figure 3**: FESEM images of (a) $Cr_2O_3$, (b) $Cr_2O_3$/CuO and (c) $Cr_2O_3$/CuO:Ni and d) EDX of $Cr_2O_3$/CuO:Ni thin film photocathode.

$Cr_2O_3$ thin films grown over the substrate exhibited a stone-like structure (figure 3a). Whereas, after being coated by CuO layer, the surface morphology of $Cr_2O_3$/CuO thin films revealed a porous surface with some large particles appeared to be a plate-like shape. The same porous structure was also recorded from $Cr_2O_3$/CuO:Ni. This structure can improve the electrode/electrolyte interfacial area. As charges are generated at the electrolyte interface, the photogenerated holes have to travel through less bulky material. As a result, chances of recombination can be reduced during the photo-oxidation reactions.[47] In the case of $Cr_2O_3$/CuO:Ni, more charges are generated than $Cr_2O_3$ and $Cr_2O_3$/CuO, thereby increasing the charge mobility. Moreover, after Ni was added in the CuO, most of the particles viewed in figure 3c) have small size compared to the particles size in figure 3b). This result was tabulated in table 1. Note that, the decrease in particle size observed in FESEM images is consistent with the XRD results calculated using Scherrer's equation. Furthermore, some of the particles seemed to agglomerate and forming rougher surface consistent with results obtained from AFM analysis. From FESEM images, the thickness of $Cr_2O_3$, $Cr_2O_3$/CuO and $Cr_2O_3$/CuO:Ni films were 0.88, 1.13 and 1.25 µm respectively (figure S1). Energy dispersive X-ray image of $Cr_2O_3$/CuO:Ni (figure 3d) confirms the elemental existence of Cr, Cu, O, and Ni.

**Optical properties**

Optical absorption measurements of $Cr_2O_3$, $Cr_2O_3$/CuO and $Cr_2O_3$/CuO:Ni thin films are shown in figure 4. Nearly similar peak pattern with the absorption peaks at ~450 and ~600 nm were observed in all samples. The similar trend of $Cr_2O_3$ absorption is also consistent with the previous study.[48] Note that, as for all samples, the dominant peak was exhibited by $Cr_2O_3$, hence the peaks of CuO and Ni cannot be seen. Initially, $Cr_2O_3$ showed moderate light intensity, however, after layers of CuO and CuO:Ni were deposited on the $Cr_2O_3$ film, the light intensity increase by ~ 10 % and ~15 % respectively. This suggests that the absorbance peaks of CuO and Ni fall in the same wavelength region of $Cr_2O_3$. Small difference in the absorption intensity of $Cr_2O_3$/CuO and $Cr_2O_3$/CuO:Ni films may be attributed to the variation in thickness as well as scattering from different morphology of the deposited films.[49]

The optical bandgap energy of the samples was estimated from Tauc plots (figure 5). The best fit for the optical bandgap was found for direct bandgap transition rather than indirect transition. The bandgap energy estimated for $Cr_2O_3$ is 3.21 eV (figure 5a). This value is smaller than previously reported for bulk counterpart (3.5 eV) [31] which can be ascribed to the quantum confinement effect.[50] It can be seen that, heterojunction $Cr_2O_3$/CuO:Ni has bandgap energy of 2.23 eV. The incorporation of CuO:Ni with $Cr_2O_3$ led to a decrease in the bandgap energy which confirm the substitution $Cu^{2+}$ ions by $Ni^{2+}$ ions in the host lattice. This facilitates an easy passage of electrons from the conduction band to the valence band as compared to the $Cr_2O_3$ sample.

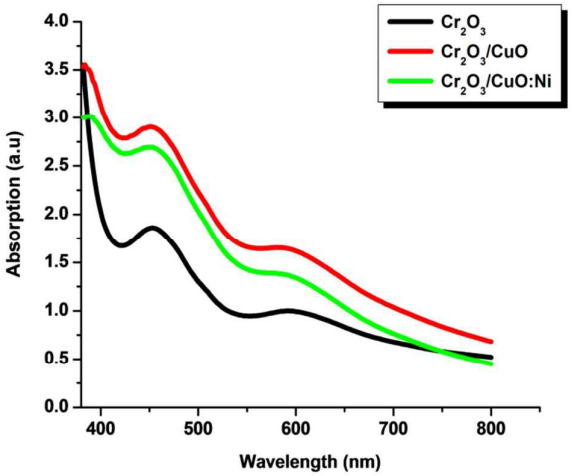


**Figure 4**: UV-Vis spectrum of $Cr_2O_3$, $Cr_2O_3$/CuO and $Cr_2O_3$/CuO:Ni thin films.

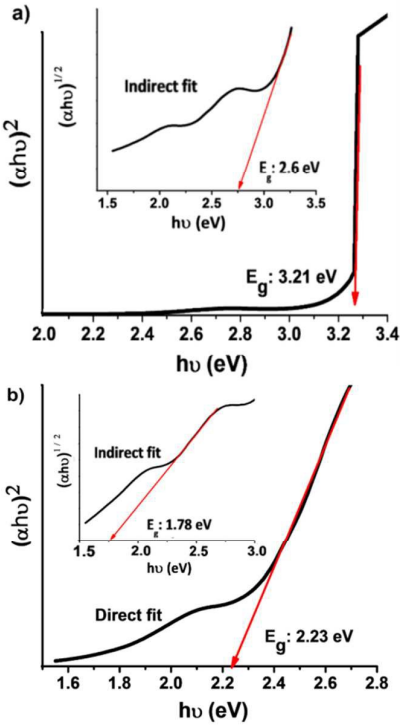


**Figure 5**: Tauc plots of a) $Cr_2O_3$ and b) $Cr_2O_3$/CuO:Ni thin films.

**PEC characterization**

The PEC performance of the thin film photoelectrodes was carried out in 0.5 M $Na_2SO_4$ electrolyte between 0.5 to -0.6 V *vs.* SCE under dark and simulated conditions. As the potentials sweep from positive to the negative direction, cathodic photocurrents are observed for all samples. Moreover, the chopped pattern displays a good initial photocurrent spike. The photocurrent spike occurs before a sharp decay to a steady-state photocurrent which generally is assigned to the electron-hole recombination at

immediate time or corrosive effects.[51] Initial experiment was carried out to determine the optimum time to deposit $Cr_2O_3$. Figure 6a) shows the time-dependence of photocurrent density of $Cr_2O_3$. $Cr_2O_3$ prepared for 30 minutes showed the highest performance with 0.1 $mAcm^{-2}$ at -0.6 V *vs*. SCE. It is known that, short deposition time result in thinner films whereas long deposition time corresponds to thicker films. As the film thickness increases, the sample produces the lowest photocurrent density. This might be due to greater distance travelled by the charge carriers, thereby, increasing the rate of recombination of electron-hole pairs.[51] On the contrary, the lowest photocurrent density recorded by the thinnest films (15 minutes) might be due to the shortest distance travelled by the charge carriers compared to its diffusion length. So, the charge carriers have not had enough time to diffuse to electron-hole pairs.

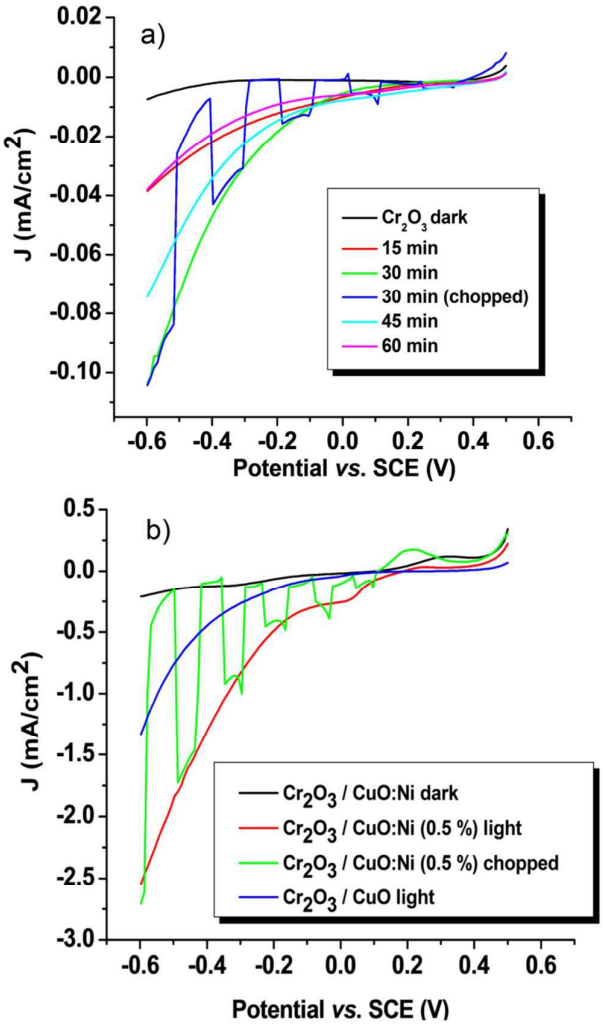


**Figure 6**: The photocurrent density-potential curves of a) $Cr_2O_3$ and b) $Cr_2O_3$/CuO:Ni (0.5 %) thin film photocathodes

The low photocurrent magnitude exhibits by $Cr_2O_3$ is due to its wide bandgap, thus limiting the electron excitation rate from valence band to the conduction band.[24] By coupling $Cr_2O_3$ with CuO forming heterojunction, the photocurrent density of $Cr_2O_3$ was increased from 0.1 to 1.33 $mAcm^{-2}$. The photocurrent enhancement is assigned to the subsequent increase of minority carriers of electrons under illumination.[51] In order to determine the improved property of $Cr_2O_3$, the photocurrent measurements of single CuO and CuO:Ni were conducted under the same condition (figure S2 and table S1). Interestingly, the results prove that the photocatalytic activity was enhanced in heterojunction structure rather than in a single-layer thin film electrode. Further, different percentage of Ni dopant was optimized in order to study its effect towards the conductivity of the prepared electrodes. Table 2 represents the photocurrent density as a function of Ni content at -0.6 V *vs*. SCE. The photocurrent density of Ni-doped CuO was enhanced as the amount of Ni increased from 0.25 to 0.5 % and then decreased with 1 % Ni. The Ni ions have similar size to $Cu^{2+}$ ions which can make it more easily substituted into CuO lattice,[5] therefore, the conductivity increased due to higher concentration of carriers available ($Cu^{2+}$ and $Ni^{2+}$). Among other samples, the $Cr_2O_3$/CuO:Ni thin film photoelectrodes exhibited higher photocurrent density of 2.6 $mAcm^{-2}$. Based on the FESEM result, it shows that the effect of Ni doping is to reduce the particles size resulting in large surface area for reaction.

**Table 2**: Photocurrent density of $Cr_2O_3$, $Cr_2O_3$/CuO and $Cr_2O_3$/CuO:Ni photocathodes with different percentage of Ni content.

| Samples | Ni content (%) | Photocurrent Density *vs.* SCE at -0.6 V ($mAcm^{-2}$) |
|---|---|---|
| $Cr_2O_3$ (30 min) | - | 0.10 |
| $Cr_2O_3$/CuO | - | 1.33 |
| $Cr_2O_3$/CuO:Ni | 0.25 | 1.42 |
| | 0.50 | 2.55 |
| | 1.00 | 1.90 |

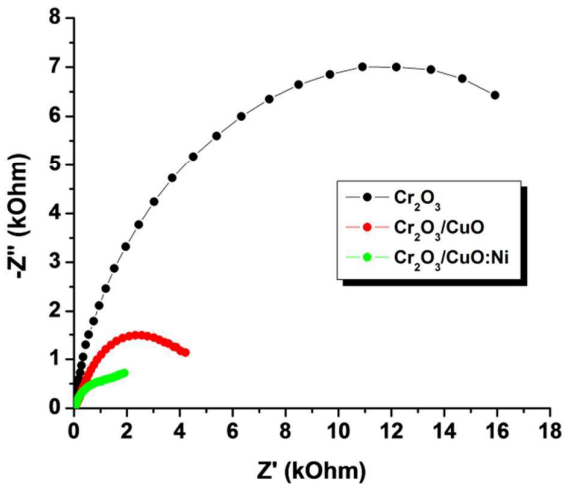


**Figure 7**: Nyquist plots of all samples under simulated 1 sun (air mass 1.5G, 100 $mWcm^{-2}$).

Electrochemical impedance spectroscopy (EIS) was carried out under illumination at bias potential -0.2 V. The characteristic of charge transfer resistance $R_{ct}$ can be represented in the semicircle of the Nyquist plot. Clearly, a smaller arc radius was observed for $Cr_2O_3$/CuO:Ni compared to those of $Cr_2O_3$ and $Cr_2O_3$/CuO (figure 7). This suggests that the charge transfer resistance of $Cr_2O_3$ was reduced due to higher electron conductivity after the formation of Ni-doped CuO heterojunction. In other words, heterojunction of $Cr_2O_3$ with CuO:Ni promotes the interfacial charge transport and facilitates the photoinduced charge separation.[52]

Mott-Schottky plots for $Cr_2O_3$ and CuO:Ni electrodes in 0.5 M $Na_2SO_4$ are displayed in figure 8a). The flatband potentials were determined from the intersection of the line fit to the $1/C^2$ with x-axis. The flatband potentials of $Cr_2O_3$ and CuO:Ni were 0.6 and 0.7 V *vs*. SCE respectively. By converting the obtained flatband potential with respect to NHE, the calculated values were 0.84 and 0.94 V *vs.* NHE. Based on the optical bandgap energy (see figure 5 and figure S3), and flatband potentials, we sketched the energy band diagram of heterojunction $Cr_2O_3$/CuO:Ni in figure 8b. The conduction band and valence band of $Cr_2O_3$ are more negative than the corresponding bands of CuO:Ni. Therefore, this condition favours the facile injection of photogenerated electrons from the conduction band of $Cr_2O_3$ to that CuO:Ni. When the photoelectrode is illuminated with simulated solar light, the photogenerated charge carriers are generated at the conduction band of both $Cr_2O_3$ and CuO:Ni. The excited electrons in $Cr_2O_3$ migrate to the conduction band of CuO:Ni easily due to the potential difference, and then accumulate with the existing photogenerated electrons of CuO:Ni. Finally these electrons move to the semiconductor/electrolyte interface whereas holes are collected onto FTO.

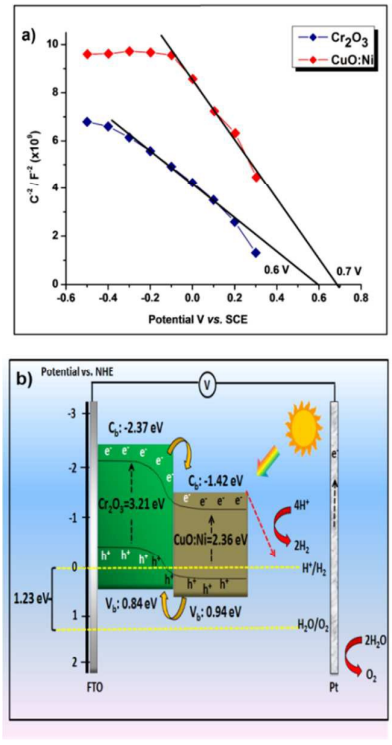


**Figure 8**: Mott-Schottky plots of a) $Cr_2O_3$ and CuO:Ni thin film photocathodes b) Schematic representation of the $Cr_2O_3$ and CuO:Ni films in aqueous medium under illuminated condition.

## Conclusion

$Cr_2O_3$, $Cr_2O_3$/CuO and $Cr_2O_3$/CuO:Ni photocathodes were successfully prepared via AACVD and spin-coating. The performance of these photoelectrodes toward PEC was studied with photocurrent density-voltage curve, EIS and Mott-Schottky analysis. The photoresponse of a single $Cr_2O_3$ photoelectrode was increased after the formation of heterojunction with CuO and Ni-doped CuO (CuO:Ni). The thin films with the composition; $Cr_2O_3$ (30 minutes), CuO layer and Ni content (0.5 %) gave the best photocurrent performance of 2.6 $mAcm^{-2}$ *vs*. SCE at -0.6 V. In a nutshell, by combining these two strategies (heterojunction and doping) in a single photoelectrode may provide an effective way to enhance the photoelectrochemical properties.

## Acknowledgement

The authors would like to thank the Universiti Kebangsaan Malaysia for the financial support from grant ICONIC-2013-005.

## Notes and references

1 S. U. M. Khan, M. Al-Shahry, and W. B. Ingler, *Science*, 2002, **27**, 2243.
2 I. S. Cho, Z. Chen, A. J. Forman, D. R. Kim, P. M. Rao, T. F. Jaramillo and X. Zheng, *Nano Lett*., 2011, **11**, 4978.
3 K. S. Ahn, Y. Yan, S. Shet, K. Jones, T. Deutsch, J. Turner and M. Al-Jassim, *Appl. Phys. Lett*., 2008, **93**, 163117.
4 C.-Y. Chiang, Y. Shin, S. Ehrman, *J. Electrochem. Soc*., 2012, **159**, B227.
5 C.-Y. Chiang, Y. Shin, S. Ehrman, *Energy Procedia*, 2014, **61**, 1799.
6 J. Lin, P. Hu, Y. Zhang, M. Fan, Z. He, C. K. Ngaw, J. S. C. Loo, D. Liao and T. T. Y. Tan, *RSC Adv*., 2013, **3**, 9330.
7 Z. Hu, M. Xu, Z. Shen and J. C. Yu, *J. Mater. Chem. A*, 2015, **3**, 14046.
8 J. S. Jang, S. M. Ji, S. W. Bae, H. C. Son and J. S. Lee, *J. Photochem. Photobiol. A,* 2007, **188**, 112.
9 Y. Tak, S. J. Hong, J. S. Lee and K. Yong, *J. Mater. Chem*., 2009, **19**, 5945.
10 S. J. Hong, S. Lee, J. S. Jang and J. S. Lee, *Energy Environ Sci*., 2011, **4**, 1781.
11 A. Fujishima and K. Honda, *Nature*, 1972, **238**, 37.
12 S. N. F. Mohd-Nasir, M. A. Mat-Teridi, M. Ebadi, J. S. Sagu, M. Y. Sulaiman, N. A. Ludin and M. A. Ibrahim, *Phys. Status Solidi A*, 2015, **212**, 2910.
13 P. Brack, J. S. Sagu, T. A. N. Peiris, A. McInnes, M. Senili, K. G. U. Wijayantha, F. Marken, and E. Selli, *Chem. Vap. Depos*., 2015, **21**, 41.
14 J. Yin, S. Huang, Z. Jian, Z. Wang, Y. Zhang, *Mater. Sci. Semicond. Process.*, 2015, **34**, 198.
15 J. A. Seabold, K. Zhu and N. R. Neale, *Phys. Chem. Chem. Phys*., 2014, **16**, 1121.
16 A. A. Tahir, M. A. Mat-Teridi and K. G. U. Wijayantha, *Phys. Status Solidi RRL*, 2014, **8**, 976.
17 R. Rajendran, Z. Yaakob, M. Pudukudy, M. S. Abd-Rahaman, K. Sopian, *J. Alloys Compd*, 2014, **608**, 207.
18 Y. S. Hu, A. Kleiman-Shwarsctein, A. J. Forman, D. Hazen, J. N. Park and E. W. McFarland, *Chem. Mater*., 2008, **20**, 3803.

19 D. K. Zhong, J. Sun, H. Inumaru and D. R. Gamelin, *J. Am. Chem. Soc*., 2009, **131**, 6086.
20 X. Liu, F. Wang and Q. Wang, *Phys. Chem. Chem. Phys*., 2012, **14**, 7894.
21 K. Sivula, F. Le Formal and M. Grätzel, *Chem. Mater*., 2009, **21**, 2862.
22 W. Cristino, S. Caramori, R. Argazzi, L. Meda, G. L. Marra and C. A. Bignozzi, *Langmuir*, 2011, **27,** 7276.
23 B. Cole, B. Marsen, E. Miller, Y. Yan, B. To, K. Jones and M. Al-Jassim, *J. Phys. Chem. C*, 2008, **112**, 5213.
24 M. Ebadi, M. A. Mat-Teridi, M. Y. Sulaiman, W. J. Basirun, N. Asim, N. A. Ludin, M. A. Ibrahim and K. Sopian, *RSC Adv.***,** 2015, **5**, 36820.
25 J. He, Y. Peng, Z. Sun, W. Cheng, Q. Liu, Y. Feng, Y. Jiang, F. Hu, Z. Pan, Q. Bian, S. Wei*, Electrochim. Acta*, 2014, **119**, 64.
26 M. A. Mat-Teridi, A. A. Tahir, S. Senthilarasu, K. G. U. Wijayantha, M. Y. Sulaiman, N. Ahmad-Ludin, M. A. Ibrahim and K. Sopian, *Phys*. *Status Solidi RRL*, 2014, **8**, 982.
27 C. Hu, K. Chu, Y. Zhao, and W. Y. Teoh, *ACS Appl. Mater. Interfaces*, 2014, **6**, 18558.
28 M. Gong, W. Zhou, M. J. Kenney, R. Kapusta, S. Cowley, Y. Wu, B. Lu, M.-C. Lin, D.-Y. Wang, J. Yang, B. –J. Hwang, H. Da*, Angew. Chem*., 2015, **127**, 12157.
29 K. Nakaoka, J. Ueyama, and K. Ogura, *J. Electrochem. Soc.*, 2004, **151**, C661.
30 Y.-F. Lim, C. S. Chua, C. J. J. Lee and D. Chi, *Phys. Chem. Chem. Phys*., 2014, **16**, 25928.
31 K. Maeda, K. Teramura, D. L. Lu, N. Saito, Y. Inoue and K. Domen, *Angew. Chem. Int. Ed*, 2006, **45**, 7806.
32 R. Bhosale, S. Pujari, G. Muley, B. Pagare and A. Gambhire, *J. Nanos. Chem*., 2013, **3**, 46.
33 J. L. Bobet, S. Desmoulins-Krawiec, E. Grigorova, F. Cansell and B. Chevalier, *J. Alloy. Compd*., 2003, **351**, 217.
34 C.-Y. Chiang, M. H. Chang, H.-S. Liu, C. Y. Tai, S. Ehrman, *Ind. Eng. Chem. Res.*, 2012, **51**, 5207.
35 C.Y. Chiang, Y. Shin, K. Aroh, S. Ehrman, *Int. J. Hydrogen Energ*., 2012, **37**, 8232.
36 C.Y. Chiang, K. Aroh, S. Ehrman, *Int. J. Hydrogen. Energ*., 2012, **37**, 4871.
37 C.Y. Chiang, K. Aroh, N. Franson, V.R. Satsang, S. Dass, S. Ehrman. *Int. J. Hydrogen. Energ*., 2011, **36**, 15519.
38 Y. S. Chaudhary, A. Agrawal, R. Shrivastav, V. R. Satsangi, S. Dass, *Int. J. Hydrogen. Energ*., 2004, **29**, 131.
39 A. Kargar, Y. Jing, S. J. Kim, C. T. Riley, X. Pan and D. Wang, *ACS Nano*, 2013, **7**, 11112.
40 S. J. A. Moniz and J. Tang, *ChemCatChem*, 2015, **7**, 1659.
41 C.-Y. Chiang, Y. Shin and S. Ehrman, *Energy Procedia*, 2014, **61**, 1799.
42 S. Al-Amri, M. S. Ansari, S. Rafique, M. Aldhahri, S. Rahimuddin, A. Azam, A. Memic, *Current Nanoscience*, 2015, **11**, 191.
43 C.-Y. Chiang, Y. Shin, S. Ehrman, *Appl. Ener*., 2016, **164**, 1039.
44 S. Al-Amri, M. S. Ansari, S. Rafique, M. Aldhahri, S. Rahimuddin, A. Azam, A. Memic, *Curr., Nano*., 2015, **11**, 191.
45 S. Baturay, A.Tombak, D. Kaya, Y.Selim Ocak, M. Tokus, M. Aydemir, T. Kilicoglu, *J. Sol-Gel Sci. Technol*., 2016, 1, 10.1007/s10971-015-3953-4
46 S. Mehraj, M. S. Ansari, Alimuddin, *J. Nanoeng. Nanomanuf*., 2013, **3**, 229.
47 S. K. Pilli, R. Janarthanan, T. G. Deutsch, T. E. Furtak, L. D. Brown, J. A. Turner and A. M. Herring, *Phys. Chem. Chem. Phys*., 2013, **15**, 14723.
48 U. Shaislamov, B. Yang and K. Park, *J. Korean Phys. Soc*., 2012, **61**, 759.
49 A. Kleiman-Shwarsctein, Y. -S. Hu, A. J. Forman, G. D. Stucky, E. W. McFarland, *J. Phys. Chem. C*, 2008, **112**, 15900.
50 H. Q. Cao, X. Q. Qiu, L. A. Yu, M. J. Zhao and Q. M. Zhu, *Appl. Phys. Lett*., 2006, **88**, 241112.
51 J. Y. Zheng, G. Song, C. W. Kim, Y. S. Kang, *Electrochimica Acta*, 2012, **69**, 340.
52 Z. Kang, X. Yan, Y. Wang, Z.Bai, Y. Liu, Z. Zhang, P. Lin, X. Zhang, H. Yuan, X. Zhang & Y. Zhang, *Scientific Reports*, 2015, **5**, 7882.